Materials Science in Semiconductor Processing 149 (2022) 106851

Contents lists available at ScienceDirect

Materials Science in Semiconductor Processing

journal homepage: www.elsevier.com/locate/mssp

New approach for the synthesis of Ag_3PO_4-graphene photocatalysts

Łukasz Lewandowski [a], Julia Zwara [a], Anna Gołąbiewska [a,*], Tomasz Klimczuk [b], Grzegorz Trykowski [c], Adriana Zaleska-Medynska [a]

[a] Department of Environmental Technology, Faculty of Chemistry, University of Gdansk, ul.Wita Stwosza 63, 80-308, Gdansk, Poland
[b] Department of Solid State Physics, Faculty of Applied Physic and Mathematics, Gdansk University of Technology, ul.Gabriela Narutowicza 11/12, 80-233, Gdansk, Poland
[c] Faculty of Chemistry, Nicolaus Copernicus University in Torun, ul.Gagarina 7, 87-100, Torun, Poland

ARTICLE INFO

Keywords:
Ag_3PO_4-graphene
Heterogenous photocatalysis
Visible light activity

ABSTRACT

A facile and effective plasma sputtering method for the preparation of a visible light active photocatalyst - rhombic dodecahedral silver phosphate Ag_3PO_4 covered with nanographene (Ag_3PO_4-GR) with improved stability has been developed. Proposed method allows for the usage of readily available materials for nanographene sputtering and for easy scaling-up. The stability improvement, confirmed by visible light-induced phenol degradation experiment, could be attributed to the synergistic effect of the silver phosphate particles and graphene material allowing for migration of metallic silver nanoparticles from semiconductor's surface to graphene body keeping the semiconductors surface "silver free". Also due to its conductive properties, nanographene may additionally be preventing electron-hole recombination and metallic silver formation.

1. Introduction

Environmental pollution is one of the most important problems that modern society has to deal with. Among other methods and technologies, visible light responsive photocatalysis, which can utilize the solar energy, is expected to play an important role in solving the urgent problem of water and air purification. In recent years, various Ag-based photocatalysts, such as Ag_3PO_4 [1–3], $AgVO_3$ [4–6], Ag_2CO_3 [7–9] and Ag_2O [10–12] have proven their promising photocatalytic performance for the degradation of organic pollutants from contaminated wastewaters, hydrogen evolution from water or Cr(VI) reduction [13,14] due to their excellent response to the visible light. Among them, silver phosphate (Ag_3PO_4) is one of the visible-light inducted photocatalysts with extremely high photooxidative capabilities for O_2 evolution in water splitting process and for the degradation of organic pollutants in aqueous solutions and possessing relatively low toxicity, as well as excellent quantum efficiency [15]. Nevertheless, the Ag_3PO_4 has an unsatisfactory stability, as it is susceptible to photo-reduction with the formation of metallic Ag, leading to deterioration of photoactivity during reaction. Thus, to overcome this limitation, the focus was on the development of a method to improve the photoactivity and stability of Ag_3PO_4. One available way is to integrate Ag_3PO_4 with other functional materials. The list of suitable materials is relatively long and includes: photocatalysts (TiO_2 CeO_2, Fe_2O_3, AgI, AgCl, ZnO etc), metal organic frameworks, carbon materials (graphene, graphene oxide and reduced graphene oxide, graphitic carbon nitride: g-C_3N_4 and carbon quantum dots) [16–18]. Graphene has been proven to be the most promising material in a wide range of applications due to a large specific surface area, high intrinsic electron mobility, good optical transparency, superior conductivity, and large adsorption capacity [19]. Integration of Ag_3PO_4 with GR sheets could increase absorption of visible light, add a transport channel for photogenerated electrons, effectively reduce photo-corrosion, and add active adsorption sites to improve photocatalytic activity of Ag_3PO_4. Based on the available literature, it could be concluded that Ag_3PO_4 and graphene composite photocatalysts could be prepared applying: (*i*) in situ growth strategy, (*ii*) liquid phase deposition, (*iii*) ion exchange - chemical precipitation method, and even (*iv*) hydrothermal method. Xiang et al. reported graphene-modified nanosized Ag_3PO_4 photocatalysts synthesized by in situ growth strategy in organic solvent and the enhanced photoactivity degradation of methylene blue (MB) under visible light irradiation [20]. Liu et at. found that tetrahedral Ag_3PO_4 with GO sheets provide an efficient solution to the photocorrosion of Ag_3PO_4. The degradation of MB reached 99% within 4 min and even after 5 cycles of photocatalytic degradation it was still as

* Corresponding author.
E-mail addresses: lukasz.lewandowski@phdstud.ug.edu.pl (Ł. Lewandowski), julia.zwara@phdstud.ug.edu.pl (J. Zwara), anna.golabiewska@ug.edu.pl (A. Gołąbiewska), tomasz.klimczuk@pg.edu.pl (T. Klimczuk), tryki@chem.umk.pl (G. Trykowski), adriana.zaleska-medynska@ug.edu.pl (A. Zaleska-Medynska).

https://doi.org/10.1016/j.mssp.2022.106851
Received 21 February 2022; Received in revised form 13 May 2022; Accepted 29 May 2022
Available online 23 June 2022

high as 97% [21]. Chen et al. developed a hydrothermal method to produce Ag_3PO_4 modified with rGO/Ag composites with high-rate photodegradation of carbamazepine under visible light [22]. However, many photocatalysts have still not evolved beyond laboratory use. Ag_3PO_4 combined with graphene via aforementioned methods has proven useful in degradation of pollutants under visible light irradiation, yet still remains viable only in a laboratory scale. For that reason, experiment in this work is focused on production of a stable, visible light sensitive photocatalyst with use of a facile and easily scalable method. Furthermore, majority of the former studies used dyes as a model contaminant to estimate visible light induced photoactivity, while dyes are not recommended to use as a model compounds, due to their large photoabsorption coefficient and complicated mechanism of degradation especially in the visible light range [23].

Herein, using graphite as a source of graphene, the composite in the form of Ag_3PO_4 wrapped by graphene layer was obtained by the plasma sputtering method. The sputtering was conducted in room temperature at the pressure of 150 mTorr with the use of readily available materials. Deep insight into correlation of sputtering time with physicochemical properties of obtained Ag_3PO_4-GR composites, demonstrates that a thin, tightly fitted yet non continuous graphene layer allows to keep the extremely high visible light induced photoactivity (λ>455 nm) and simultaneously enhance stability of this photocatalyst. Unexpectedly, TEM analysis revealed the presence of 10 nm silver nanoparticles incorporated into graphene flakes covering Ag_3PO_4 particles, probably originating from the reduction of Ag^+ in Ag_3PO_4 occurring at the time of plasma sputtering process. Then, we studied its visible light responsive photocatalytic activity on the degradation of phenol in aqueous solution. Further, we investigated the influence of graphene content on the photocatalytic activity of as-prepared composite photocatalyst. This new hybrid photocatalyst is anticipated to open new possibilities in environment remediation using solar energy.

2. Experimental

2.1. Materials and preparation of Ag_3PO_4

All the reagents were of analytical purity and used as received. The silver nitrate (98%, Sigma-Aldrich) was used as a precursor of silver in synthesis of silver phosphate. polyvinylpyrrolidone (PVP), (M_W = 300,000), sodium dihydrogen phosphate dihydrate ($NaH_2PO_4{\cdot}2H_2O$, 99%) were purchased from Sigma Aldrich. 7.9 g PVP was dispersed in 200 ml of deionized water. In the next step 4.25 g of $AgNO_3$ was dissolved in 100 ml of deionized water and was added to the PVP solution. Then Na_2HPO aqueous solution (5.68 g in 200 ml) was added dropwise, while stirring until the solution became yellow in color. Obtained material was centrifuged and flushed with deionized water and ethanol several times, next step was vacuum drying at 60 °C [3]. The synthesis follows subsequent formulas:

$$AgNO_3 \rightleftharpoons Ag+ + NO_3^-$$

$$H_2PO_4 \rightleftharpoons HPO_4^{2-} + H+ \rightleftharpoons PO_4^{3-} + 2H^+$$

$$PO_4^{3-} + 3Ag^+ \rightarrow Ag_3PO_4$$

2.2. Nanographene deposition on Ag_3PO_4

The nanographene deposition on Ag_3PO_4 was performed by plasma sputtering. The operation was done in a glass reactor with a stainless-steel substrate electrode (positive) and graphite target electrode (negative). The sputtering was conducted at the pressure of around 150 mTorr with 2000 V. 0.3 g of Ag_3PO_4 was evenly distributed upon a tray of 1.5 cm radius and placed 3 cm from the target electrode, next the vacuum pump was activated and after achieving 150 mTorr, the voltage was applied for a selected time, specific for each sample: 15, 30, 60, 150 and 300 s. Then the sample was mixed until it gained homogenous color and put back on the sample tray. After that the sputtering process was repeated. Each sample underwent three cycles total. The reactor schematic is presented in Fig. 1. Such process was expected to cover the substrate (in this case Ag_3PO_4) with small graphene flakes exfoliated from the graphite target electrode. Thus, henceforth the produced coating is referred to as nanographene in this paper.

2.3. Characterization

Raman spectra were measured with Thermo Fisher scientific DXRtm3 Spectrometer. Samples were measured in the form of pellets, with a 532 nm laser. TEM results have been obtained with the use of a transmission electron microscope by FEI Europe, model Tecnai F20 X-Twin. Measurements were made in transmission electron microscopy (TEM) and scanning transmission electron microscopy (STEM). In TEM mode, a dark field (DF) detector was used for imaging. In the STEM mode, a high angle annular dark field (HAADF) detector was used for imaging, and energy dispersive spectrometer (EDS) was used to analyze the elements. SEM images were collected with the use of JEOL JSM 7000 scanning electron microscope. Powder X-ray diffraction (pXRD) analysis on well-ground powder of samples was carried out on a Bruker D2 Phaser diffractometer with Cu Kα radiation and a LynxEye-XE detector. UV-VIS DRS (Diffuse reflectance spectra of the samples were collected with a UV 2600 Shimadzu UV-VIS spectrophotometer with $BaSO_4$ as reference.

2.4. Photocatalytic tests

The photoactivity of the samples was evaluated by the means of phenol degradation under visible light using a 1000 W Xenon lamp along with 455 nm cut-off filter. The irradiation intensity was measured using a hand-held meter made by Hamamatsu, model C9536-01 and reached 3 mW/cm^2 at the surface of the reactor. 125 mg of photocatalyst was added to 25 ml of aqueous phenol solution of 0.21 mM concentration. The mix was placed in a photoreactor with a quartz window and stirred throughout the whole process. The irradiation was preceded by 30 min of darkness to achieve sorption/desorption equilibrium. Blind test (phenol solution with no photocatalyst) was performed showing 2% loss of phenol over the period of 60 min. Four 1 ml samples were taken in the interval of 5 min through 20-min irradiation cycles. For a better insight of the photoinduced processes, benzoquinone evolution was evaluated along phenol degradation, as it is phenol's degradation by-product. Phenol and benzoquinone concentration were estimated by high performance liquid chromatography (HPLC, Shimadzu). The HPLC system was equipped with a Kinetex C18 column (150mm × 3 mm; particle size of 2.6 μm; pore diameter 100 Å). Flow rate was maintained at 0.4 ml/min with acetonitrile and water mix, 7.7 to 92.5 volumetric proportion respectively. Sample injection volume was 30 μl. SPD-M20 A diode array detector operating at 205 nm was utilized.

2.5. Action spectra

Action spectra (AS) experiments were performed for pristine Ag_3PO_4 and also for the most stable sample – Ag_3PO_4_GR(15s). Degradation of phenol and subsequent evolution of hydroquinone under monochromatic light was investigated. Six wavelengths were selected for the experiment (455, 460, 470, 480, 505, 510) corresponding to photon energy range 2.72 to 2.43 eV. JASCO, RM DF diffraction gating illuminator was used in tandem with a 1000W Xenon lamp (Hamatsu, C2578-02). 25 mg of the sample was placed in a quartz reactor filled with 15 ml of 20 mg dm^{-3} phenol solution and subsequently irradiated with a given wavelength for a period of 1 h. After that, phenol concentration was determined with HPLC. Light intensity was measured by HIOKI 3664 power meter. Each experiment was accompanied by a 'blank' sample –

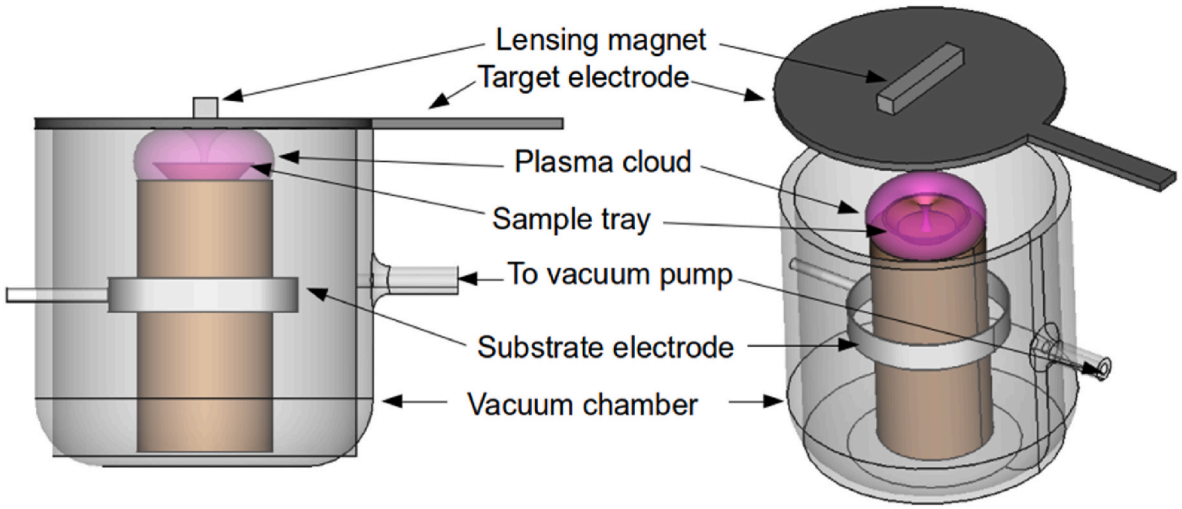

Fig. 1. Scheme of the laboratory scale plasma sputter reactor.

only phenol solution with no photocatalyst. All samples were magnetically stirred throughout the whole process.

2.6. Scavengers

Investigation on the involvement of active species was done by adding the scavengers of radicals to the photocatalytic reaction The procedure was the same as described for phenol degradation with the exception that scavengers were present in the solution. Each scavenger was investigated separately and its concentration was set to 0.21 mmol dm^{-3}. Three types of scavengers were investigated – p-Benzoquinone (BQ) as a superoxide scavenger ($O_2^{-\bullet}$), *tert*-Butyl alcohol (TBA) as hydroxyl scavenger ($^{\bullet}OH$), and $AgNO_3$ as electron scavenger (e^-). The experiment was set to replicate that of previous work on Ag_3PO_4 with different morphologies [3] to allow better comparison of the results and identifying potential differences in reaction mechanisms due to introduction of graphene.

3. Results and discussion

3.1. Morphology, EDS and HAAFD

Sample labels and details of the synthesis time have been listed in Table 1. The morphology and size distribution of Ag_3PO_4 and Ag_3PO_4_GR particles were investigated using SEM. Typical SEM image of Ag_3PO_4 nanoparticles obtained via a hydrothermal method is shown in Fig. 2a. The size of Ag_3PO_4 particles was ranging from 0.5 to 10 μm. The individual particles were of irregular shape with smooth surfaces. Exposing Ag_3PO_4 to nanographene deposition via plasma sputtering process had a very prominent effect on its morphology. As the particles remained the same size, their surface underwent a very visible change. The correlation between morphology and plasma sputtering time was observed, with increasing plasma sputtering time, Ag_3PO_4 lost its smoothness and became rough. Moreover, in various places graphene-like material appeared as semi-transparent flakes sticking to the Ag_3PO_4 (Fig. 2). Work by other authors demonstrated morphology of pure Ag_3PO_4 mostly similar to the one in the current experiment [21–26]. In current work, plasma sputtering yielded no big structures. Creating only relatively small flakes and surface deformations different from typical metallic Ag deposits visible on Ag_3PO_4 in previous experiments by other authors (Fig. 2) [25,27–30].

Table 1
Sample labels, sputter times and activity.

Sample label	Sputter time (s)	Phenol degradation after 10 min irradiation (λ > 455 nm) (% degraded phenol)
Ag_3PO_4	0	100
Ag_3PO_4_GR (15s)	15	84
Ag_3PO_4_GR (30s)	30	67
Ag_3PO_4_GR (60s)	60	72
Ag_3PO_4_GR (150s)	150	81
Ag_3PO_4_GR (300s)	300	23

TEM images showed Ag_3PO_4 covered in graphene flakes, harboring particles of metallic silver as small as 10 nm in diameter in all investigated samples. The metallic silver nanoparticles, present in the samples, most probably originated from the reduction of Ag^+ in Ag_3PO_4. Plasma sputtering process does expose Ag_3PO_4 to ion bombardment and high temperatures to some degree, which can trigger the reduction of silver, also photocatalytic process induces photocorrosion of Ag_3PO_4 thus further increasing the count of metallic silver in the material. Samples with short sputtering time (15 s) seemed to have the graphene flakes more tightly fitted to the surface of Ag_3PO_4 while longer sputter times produced bigger and more discrete flakes, protruding from the silver phosphate matrix. Elemental composition by EDS analysis demonstrated that primary samples were mostly comprised of carbon, silver, oxygen, and phosphorus (Fig. 3). Which was consistent with the expected sample composition. STEM-EDS technique confirmed the presence of a graphene matrix comprised predominantly of carbon (Fig. 4 and Fig. 5), against which metallic silver nanoparticles stand out. The feature was visible both surface-wise and on mapping (Fig. 4) and line scan (Fig. 5). It is important to note that the obtained product should not be confused with Ag_3PO_4 fully encapsulated in graphene as there are discontinuities in the nanographene layer and the semiconductor still has direct contact with the ambient environment.

3.2. UV-VIS spectroscopy and Raman analysis

The UV–vis diffuse reflectance spectra of all samples are demonstrated in Fig. 6 a). Pure Ag_3PO_4 presented prominent absorption properties in both the UV and visible regions range shorter than 550 nm. For Ag_3PO_4 subjected to plasma nanographene sputtering process, a significant increase of absorbance in the visible light region (>560 nm) has been observed. The obtained results indicate that the pure Ag_3PO_4 and Ag_3PO_4-GR samples are appropriate for use as visible light induced photocatalysts. Absorption spectra of Ag_3PO_4 subjected to plasma

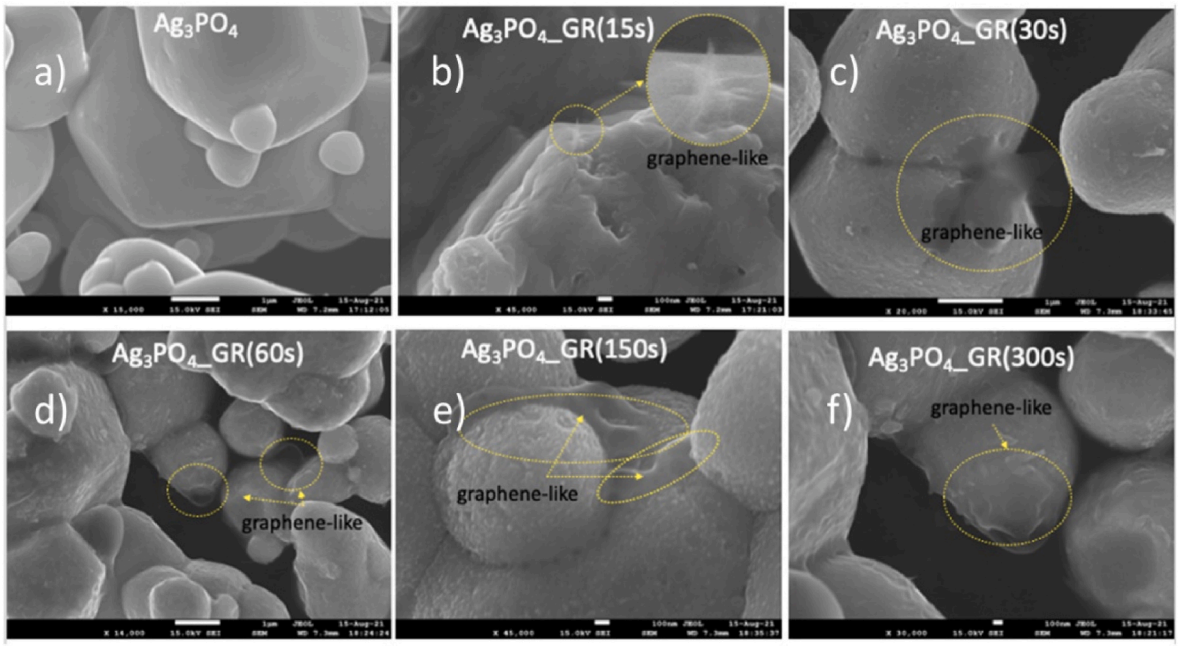

Fig. 2. SEM images of photocatalyst samples, graphene-like material was marked with circles: (a) pristine Ag_3PO_4; (b–f) Ag_3PO_4 covered by graphene through sputtering from 15 to 300 s.

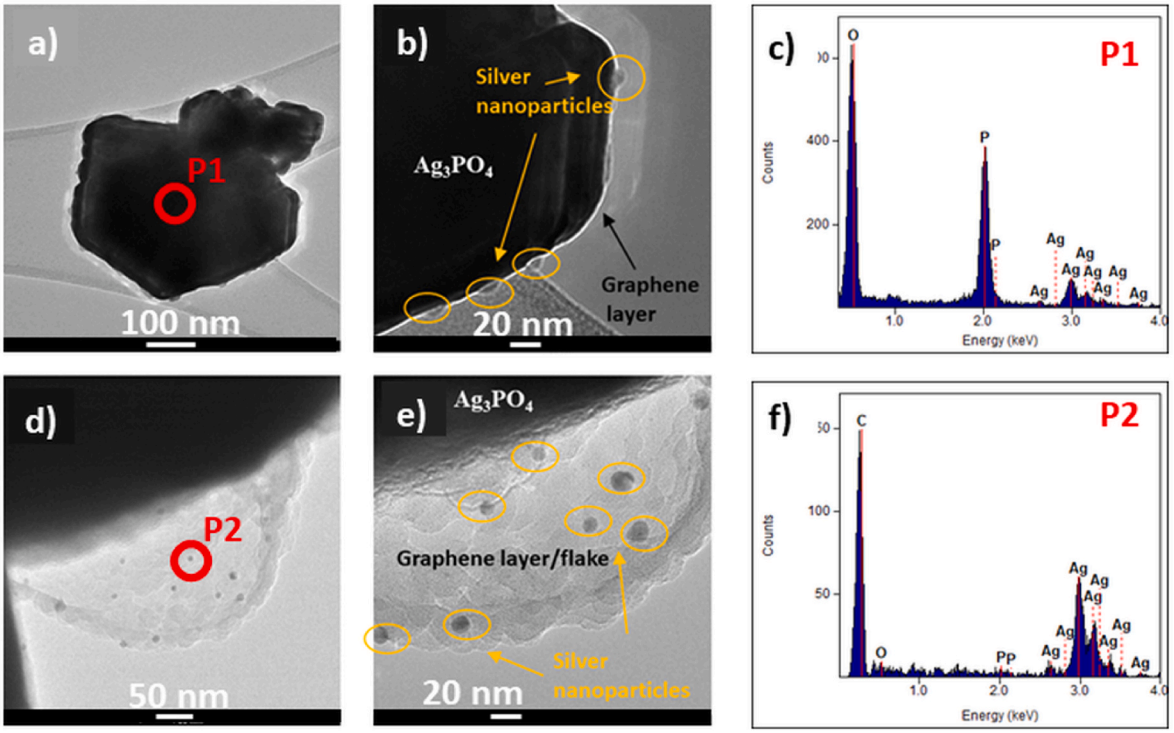

Fig. 3. TEM results: (a–c) Ag_3PO_4_GR(15s) sample after photocatalytic process and (d–f) Ag_3PO_4_GR(150s); (a, b, d, e) TEM images; (c, f) EDS spectra P1, P2, marked in red circle. Metallic silver nanoparticles have been marked in golden circles.

nanographene sputtering were similar to those of Ag_3PO_4-graphene and Ag_3PO_4-graphene oxide composites as reported by other researchers [25,26,28].

Fig. 6 b) presents Raman spectra of investigated samples. All samples demonstrated typical Ag_3PO_4 peaks at ~406 cm^{-1} (symmetric bending of the [PO_4]), 555 cm^{-1} (asymmetric bending of [PO_4]), and 909 cm^{-1} (symmetric stretch of O–P–O bonds), and 1003 cm^{-1} (asymmetric stretch of O–P–O bonds) [25,27,31–36]. Additionally, the strong absorption peak at ~909 could be attributed to the motion of terminal oxygen bond vibration of its phosphate group. The characteristic peak at 1580 cm^{-1} of graphene was also visible in all the samples. This result was in unison with highly oriented pyrolytic graphite G band which is corresponding to the in-plane sp2 hybridized carbon atoms of graphene or graphite [35–38]. The absence of D peak testified to a lack of the edge defects of graphene planes and the degree of orderliness of structure or was simply too small to be distinguishable from background noise. The

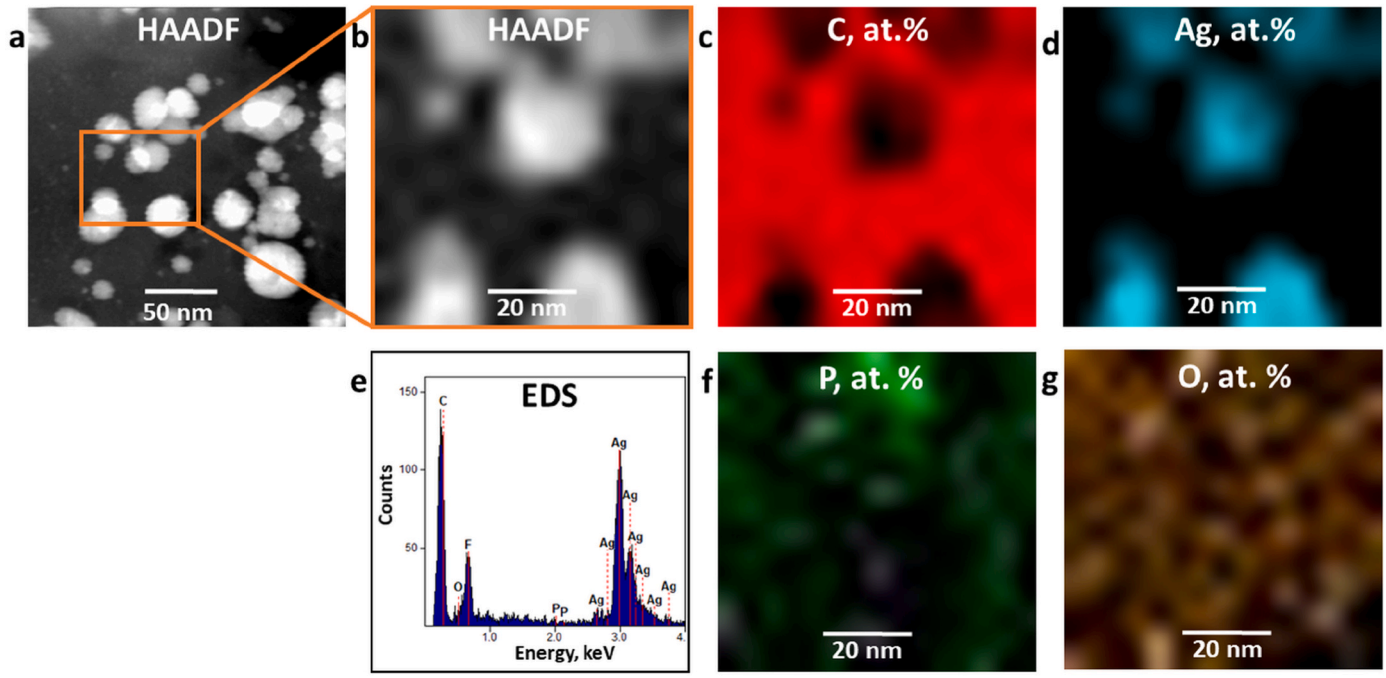

Fig. 4. TEM results: Ag nanoparticles in graphene matrix in Ag_3PO_4_GR(150s) sample, (a, b) STEM-HAADF imaging, (c, d, f, g) maps of elements, (e) EDS spectrum.

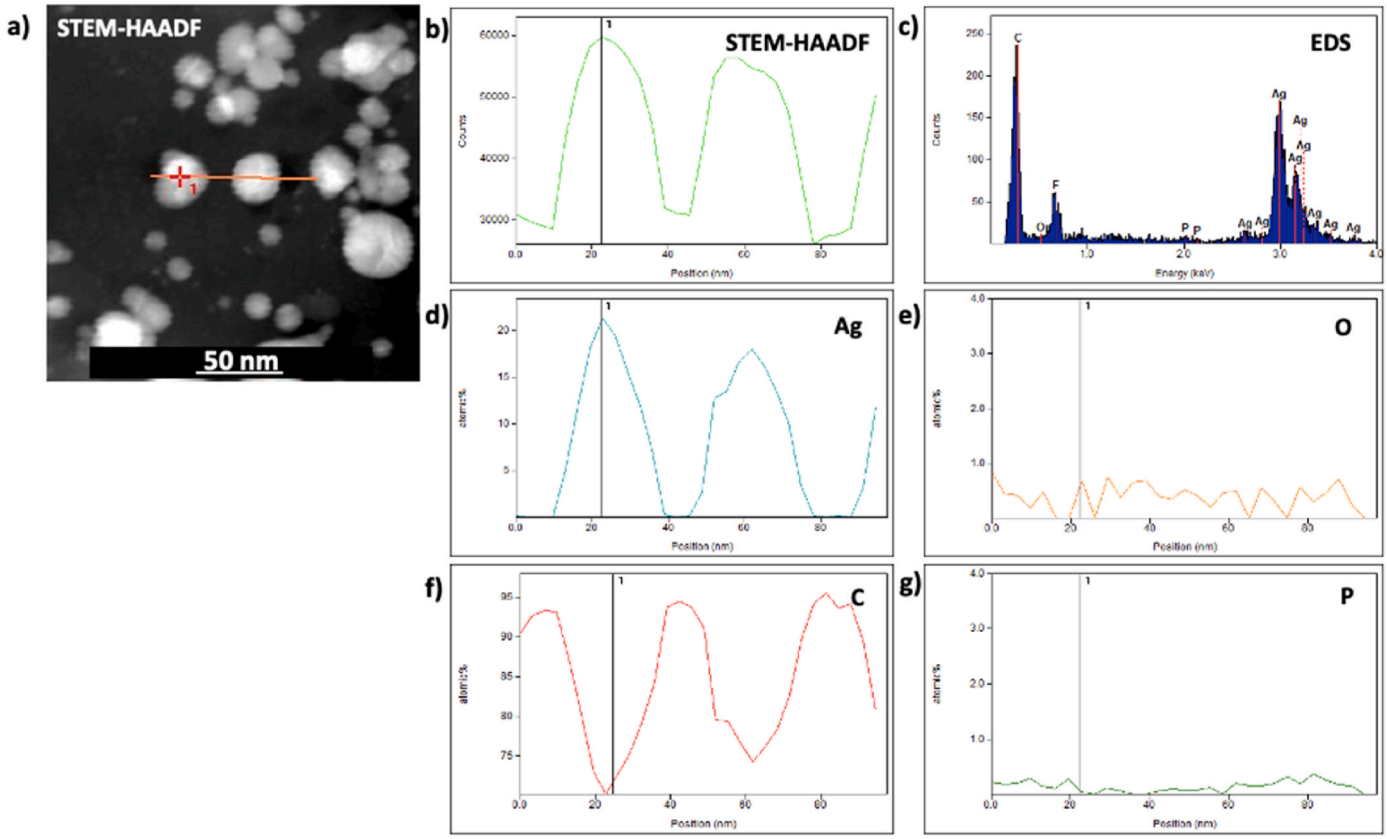

Fig. 5. TEM results: line scan of Ag nanoparticles in graphene matrix in Ag_3PO_4_GR(150s) sample; (a) STEM-HAADF imaging, (b) STEM-HAADF histogram, (c) EDS spectrum, (d–g) profiles of elements.

G band peak intensity didn't clearly depend on the sputtering time. Just after 15 s of sputtering, the G band was already prominent and didn't change much throughout the samples, except for Ag_3PO_4_GR(300s) where the peak was obscured by background noise generated by the accumulation of soot. A possible explanation is that the sputtered graphene, although increasing in abundance with the sputter time, does not really change its properties until the time of sputtering is long enough for soot (or other form of amorphous carbon) to build up and obscure it.

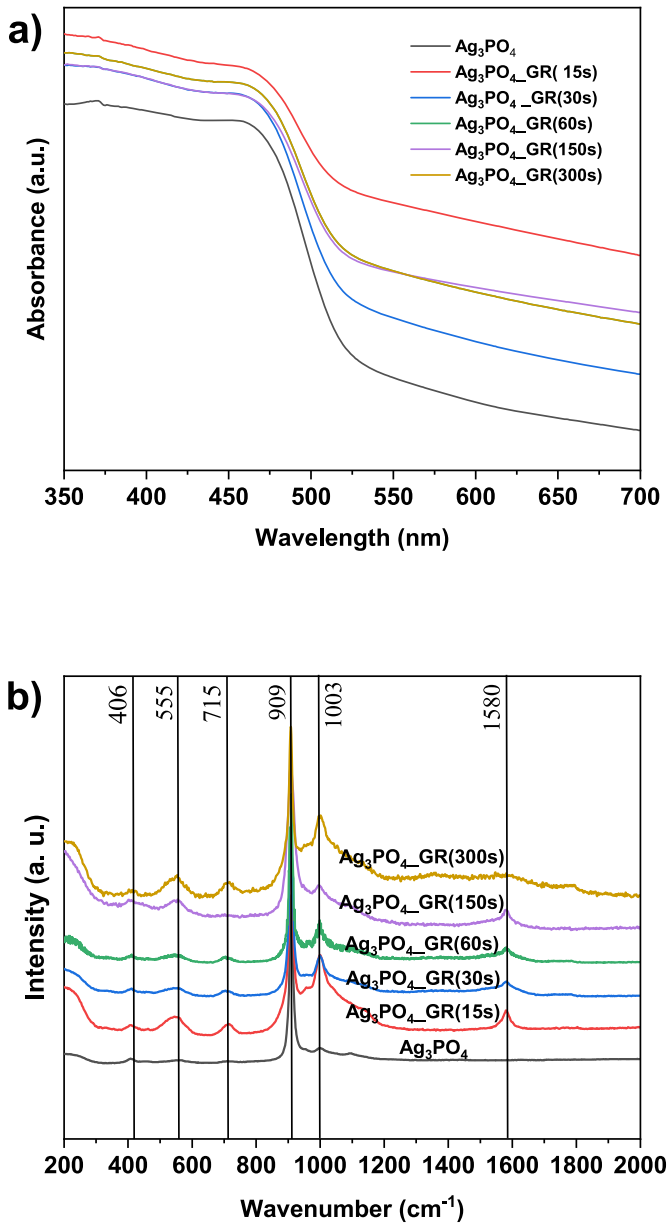

Fig. 6. a) UV-VIS spectra of the obtained samples b) Raman spectra of: Ag_3PO_4; Ag_3PO_4_GR(15s); Ag_3PO_4_GR(30s); Ag_3PO_4_GR(60s); Ag_3PO_4_GR(150s) and Ag_3PO_4_GR(300s).

3.3. XRD analysis

X-ray diffraction patterns confirm the initially obtained material to be Ag_3PO_4 as peaks at 20.9°, 29.7°, 33.2°, 36.6°, 47.8°, 52.7°, 55.0°, 57.3°, 61.6°, 69.8° and 71.9°, can be indexed by the crystallographic (110), (200), (210), (211), (310), (222), (320), (321), (400), (420), (421) planes assuming a cubic (P-43n) crystal structure type. The refined lattice parameter a = 6.0127(2) Å is very close to a = 6.01839(7) reported value for Ag_3PO_4 [38]. The base material and samples exposed to plasma sputtering did not show traces of metallic silver, unlike the post-process samples, where reflections at 38.1, 44.3 and 64.4 respectively corresponding to (111), (200) and (220) planes appeared (Fig. 7). This effect is likely to be caused by a fact that silver in Ag_3PO_4 is very susceptible to thermal and photoinduced reduction to metallic form. The nanographene deposition method used in this work was specifically custom selected for this material as it allows for graphene nanostructures deposition without significantly heating up the sample. The

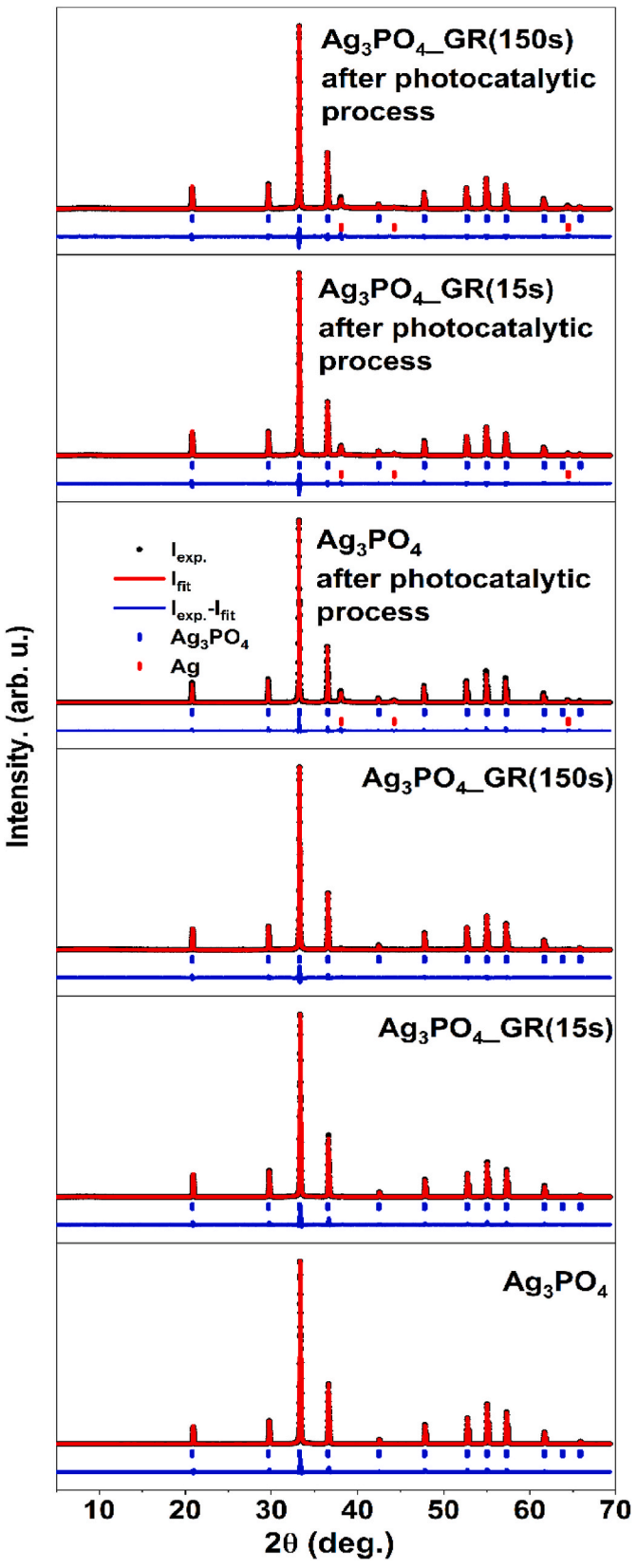

Fig. 7. Power X-ray diffraction patterns for: Ag_3PO_4, Ag_3PO_4_GR(15s), Ag_3PO_4_GR(150s), before and after the photocatalytic process of phenol degradation.

ambient plasma, carries little heat due to very low density (similar to ionosphere layer of the atmosphere). No traces of graphene in obtained diffraction patterns were observed in the Ag_3PO_4-GR, possibly due to very low concentration.

3.4. Photocatalytic properties

The effect Ag_3PO_4 modification by graphene plasma sputtering has on photoactivity, was determined by Vis light induced phenol decomposition experiment. The results of the experiment are presented in Fig. 8. The experiment was superseded with a blank test that proved that phenol decomposition in absence of the photocatalyst is below 2% and thus can be neglected. Pure Ag_3PO_4 has proven to be the most active sample with all the phenol decomposed below 5 min into the test. During that time, benzoquinone reached the level of 0.5 mg/L and remained at this concentration until the end of the trial. The second most active sample was the one exposed to plasma sputtering for 15 s (Ag_3PO_4_GR(15s)). In this case, phenol concentration dropped approx. 90% after 5 min of irradiation, and after 10 min phenol decomposed completely. Benzoquinone concentration kept on rising throughout the whole time of irradiation, reaching over 0.8 mg/L at the end of the cycle and hinting that some photocatalytic processes may be in operation even

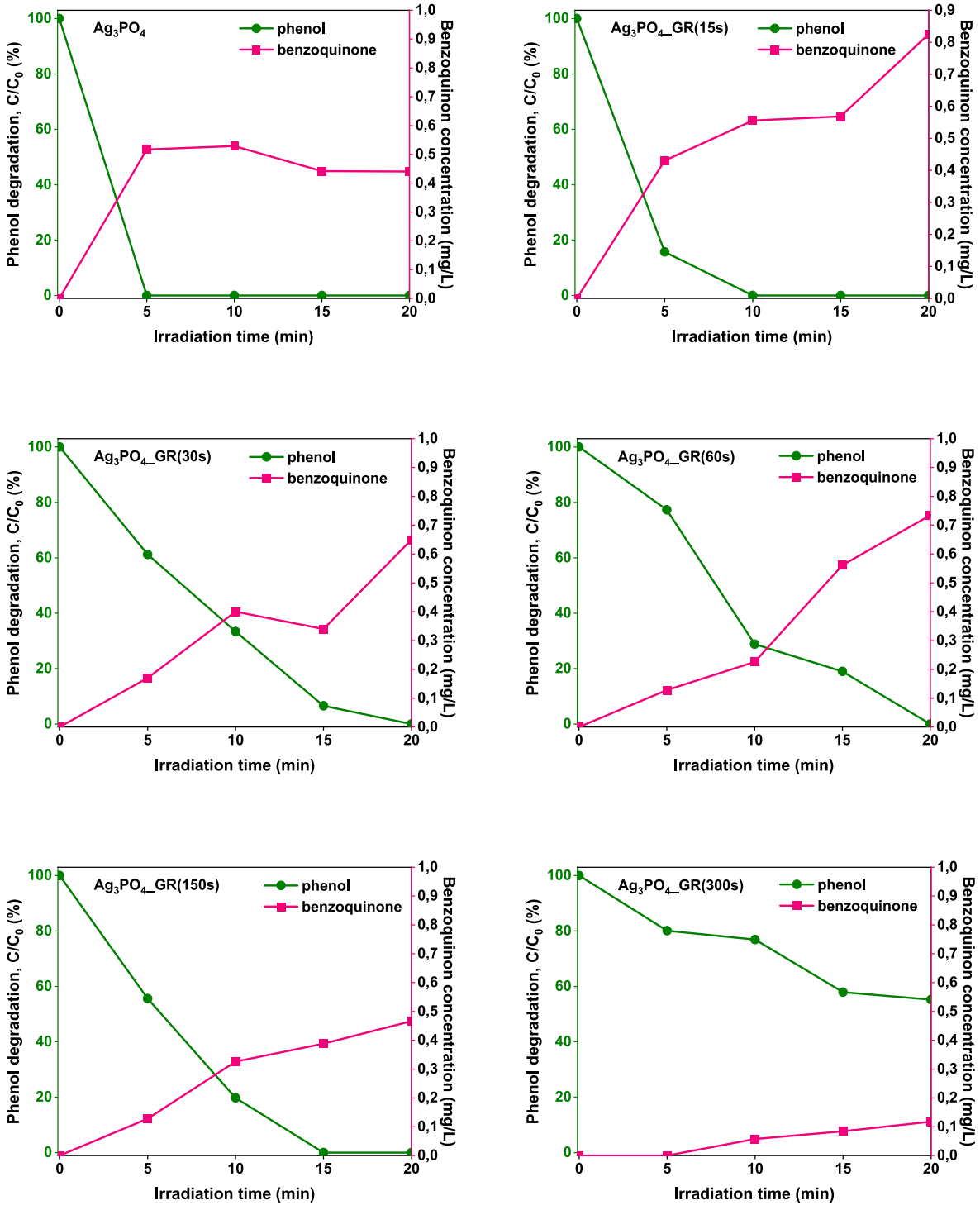

Fig. 8. Kinetics of benzoquinone evolution and phenol degradation under visible light irradiation.

after phenol has depleted. Samples Ag_3PO_4-30sec, Ag_3PO_4-60sec and Ag_3PO_4-150sec yielded similar results with the phenol mostly decomposed after 15 min of irradiation and benzoquinone steadily increasing in concentration over 20 min of the experiment. The Ag_3PO_4-300sec sample has proven the least photoactive with phenol degraded only by around 50% over 20 min, accompanied by a very small rise of benzoquinone only to a little over 0.1 mg/L in the same time.

The most active graphene modified sample was also the one with the highest light absorption coefficient (Ag_3PO_4_GR(15s), much higher than pristine Ag_3PO_4. Precise comparison of photoactivity of samples from current work to experiments reported in recent literature is difficult due to vastly different experimental procedures and equipment. However, based on data gathered in Table 2, it could be stated that us-prepared sample, obtained by 15 s sputtering by graphene, shows very high efficiency in phenol degradation, comparable to that reported for other samples, notwithstanding, us-prepared sample revealed photoactivity for wavelength longer than 455 nm, while more energetic light (λ>420 nm) was used for others.

3.4.1. Stability

Ag_3PO_4, being a very promising photocatalyst, has a certain flaw which is its tendency to degradation. Three selected samples have been tested for stability over the course of four photodegradation cycles. As demonstrated in Fig. 9, pure Ag_3PO_4 was unstable and underwent almost full degradation with only 5% of its original efficiency remaining after the experiment. Fifteen seconds of exposure to nanographene plasma sputtering dramatically improved the stability of the photocatalyst with almost 70% of its initial efficiency remaining intact after 4 cycles of use. Surprisingly, 150 s exposure to the same process did not improve the stability further but decreased it in relation to the 15 s counterpart. The main reason for Ag_3PO_4 instability is the tendency of photo-induced electrons to reduce Ag^+ to metallic silver, according to the reaction:

$$4\ Ag_3PO_4 + 6\ H_2O + 12\ h^+ + 12e^- \rightarrow 12Ag + 4H_3PO_4 + 3O_2$$ [39,40]

As demonstrated by previous experiments, modification of Ag_3PO_4 with graphene-based nanomaterials can suppress electron-hole recombination and increase adsorption of pollutants leading to increased decontamination properties [41,42], further, Graphene or graphene-oxide can act as electron relay and thus prevent the reduction of silver, in effect halting the aforementioned reduction and enhancing the stability of the material. The enhancement of stability and photoactivity of Ag_3PO_4 is usually attributed to surface modification with conductive materials like graphene or metals [26–28,30,33,34,43–45]. One of noteworthy mechanisms of Ag_3PO_4 stability and activity improvement methods is annealing, which leads to creation of metallic nanoparticles and oxygen vacancies in Ag_3PO_4 crystal structure, thus improving stability and activity respectively as metallic silver is a conductor and acts similarly to graphene by relaying electrons and thus preventing Ag^+ reduction, while crystal structure defects act as active sites increasing photoactivity [45]. Plasma nanographene sputtering process, designed to be as gentle for Ag_3PO_4 as possible, causes nanographene flakes (conductor) deposition on the surface of the semiconductor, thus increasing its stability. Also, if the sputtering process lasts less than 20 s it does not distort the crystal structure and in effect has little impact on the activity. TEM analysis of the samples before and after photocatalytic process revealed, that before the process started, only few silver nanoparticles were observed about 10 nm in size (Fig. S1 supplementary information). On the other hand, after irradiation the number and size of silver nanoparticles increased significantly, which may be related to the reduction of Ag^+ ions on the surface to the Ag^0 form [47]. The obtained results are consistent with the XRD analysis, in which a characteristic silver diffraction peak was observed for the samples after the photocatalytic process (Fig. 7). These results indicate that, in this case, plasma graphene sputtering does not entirely prevent the reduction of Ag^+, most probably because either the graphene coating does not cover the entire surface of the semiconductor particles or the light penetrating the nanographene cover can still induce photocorrosion. Yet graphene does increase the photocatalyst's stability. A noteworthy fact is that many of the observed Ag^0 nanoparticles were not situated directly on the surface of the semiconductor, but rather migrated onto the graphene body, thus losing direct contact with Ag_3PO_4 which may terminate the process of aggregation of individual silver nanoparticles and help keep the semiconductor's surface unshielded from the ambient environment. Migration of silver nanoparticles on graphene oxide and other carbon nanostructures has been observed before [46,47] but was never considered a possible stability-increase mechanism.

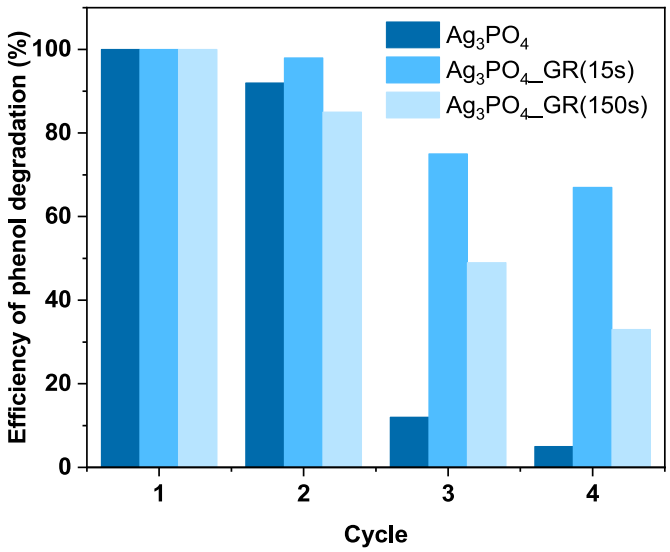

Fig. 9. Stability experiment results.

3.4.2. Action spectra

In order to determine if graphene plasma sputtering has any influence on the correlation between photoactivity and the irradiation wavelength, pristine Ag_3PO_4 and the most stable sample - Ag_3PO_4_GR (15s) were investigated for action spectra analysis. The apparent quantum efficiency (AQE) was calculated as a function of irradiation light (455, 460, 470, 480, 505, 510 nm) and is defined in the following equation:

Table 2
Juxtaposition of the results of model compounds photodegradation in the presence of Ag_3PO_4-based photocatalysts modified by carbon materials – current work vs. previous experiments.

Semiconductor	Modifier	Irradiation source	Model compound	Irradiation time	Initial conc. (mg •dm^{-3})	Cut off filter (nm)	C/C$_0$ (Approx.)	Ref.
Ag_3PO_4	GO	Halogen 500W	phenol	5 h	10	420	0.5	42
Ag_3PO_4	GO	Xenon 300W	phenol	10 min	10	420	0	54
Ag_3PO_4	GR	Xenon 350W	phenol	5 min	8	420	0.1	76
Ag_3PO_4	GR	Xenon 1000W	phenol	10 min	20	455	0.16	current work

$$AQE(\%) = \frac{2 \times \mathbf{numberofevolvedhydroquinonemolecules}}{\mathbf{numberofincidentphotons}} \times 100\%$$

The results of the experiment have been presented in Fig. 10. Action spectra analysis revealed that, as the incident wavelength increases, the AQE decreases for pristine Ag_3PO_4 and Ag_3PO_4_GR(15s) photocatalysts. Sample exposed to plasma sputtering appears less active than pristine Ag_3PO_4 in the shorter wavelength range (455, 460 nm) but becomes more active than pristine Ag_3PO_4 in the longer wave range (505, 510 nm). The AQE of samples shows a good overlap between the apparent quantum efficiencies and absorbance spectrum at different irradiation wavelengths. Thus, photocatalytic degradation of phenol was mainly dependent on the photoabsorption properties of the used photocatalyst.

3.4.3. Scavengers

For a better insight into the reaction mechanism, an experiment with the presence of scavengers of radicals has also been performed for the most active sample (Ag_3PO_4_GR(15s)). The effect of the active species experiment detailed results can be seen in Fig. S2 (supplementary information). Obtained results allow for a better insight into the photocatalytic reaction pathways and are congruent with previous work by Zwara et al. [3], confirming the primary role of $O_2^{-\bullet}$ in the degradation of phenol process. Autors confirmed that hydroxyl radicals are not abundantly generated and thus don't play the key role in the reaction and proposed that visible light photoactivity of Ag_3PO_4 may partly emerge from excited metallic particles due to surface plasmon resonance (SPR) and next electron transfer from the metal nanoparticles to the conduction band of the semiconductor. Similarity of ours and Zwara's results indicates that same mechanism is responsible for the photoactivity of Ag_3PO_4_GR and the presence of nanographene does not impact the photocatalytic mechanism itself, which could explain why no significant photoactivity increase was observed.

4. Conclusion

In this paper we demonstrate a versatile method of obtaining nanographene-modified semiconductors. The proposed method can be used to prepare a diversity of materials such as: semiconductors, metals, and insulators, additionally has the advantages of simple equipment, easy control. large coating area and strong adhesion. Presence of graphene in the as prepared samples has been confirmed by three different techniques – SEM and TEM imaging and Raman spectroscopy. Nanographene sputtered samples have proven to gain much higher stability in a photocatalytic process than pure Ag_3PO_4, although photocorrosion wasn't entirely eliminated. There is a strong inverse correlation between Ag_3PO_4 stability and plasma sputtering time, which is not clearly reflected in morphology and other measured properties of the samples – hinting a yet to be experimentally identified characteristic underlaying the stability gain mechanism. The mechanism of Ag_3PO_4 deactivation due to silver reduction has been described before – the process starts with initial increase of photoactivity due to appearance of metallic silver which prevents electron – hole recombination, but as silver accumulates, the photoactivity gain is eventually hindered by excess of metallic Ag that blocks the light and insulates the photocatalyst from the environment [48]. Presence of sputtered graphene may alter that process by allowing Ag nanoparticles to migrate onto the graphene body and thus helping to keep the semiconductor's surface uncovered. Also, effects of graphene modification introduce a large built in potential in the Ag_3PO_4-graphene interface enabling charge transfer from the semiconductor to graphene in the ground state and thus preventing the reduction of Ag to metallic form [49].

We propose that the increased stability of Ag_3PO_4 observed in this work, is due to effect of graphene, allowing the migration of metallic silver nanoparticles from the surface of Ag_3PO_4 thus unblocking its surface and also working as a charge relay thus attenuating the rate of Ag^+ reduction and simultaneously increasing photoactivity of the sample in the longer wavelengths (As demonstrated by action spectra analysis). While the excess of sputtered nanocarbon and accumulation of metallic silver during prolonged plasma sputtering and photocatalytic process may lead to blocking the light and deterioration of photoactivity. The overall properties of investigated photocatalytic materials are the net effect of the abovementioned processes.

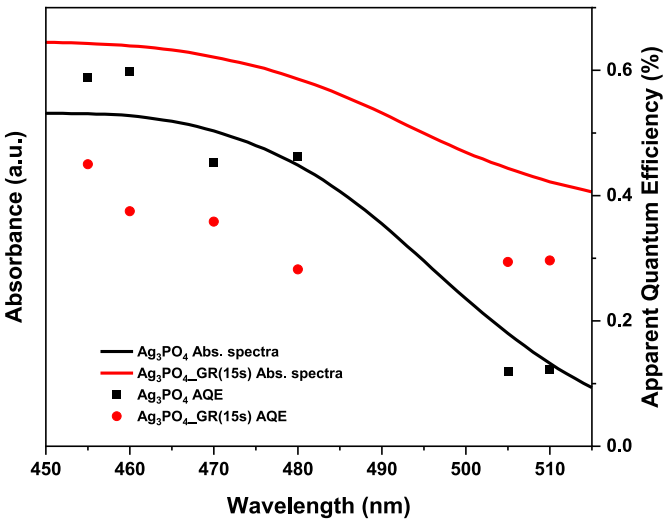

Fig. 10. Action spectra of pristine Ag_3PO_4 and Ag_3PO_4_GR(15s) Absorption spectra of Ag_3PO_4 and Ag_3PO_4_GR(15s) has been presented as black and red lines respectively. Apparent Quantum Efficiency (AQE) has been presented as black squares for Ag_3PO_4 and red dots for Ag_3PO_4_GR(15s).

Funding

This research received no external funding.

Data availability statement

All data available upon request from corresponding author.

CRediT authorship contribution statement

Łukasz Lewandowski: Writing – original draft, Visualization, Validation, Methodology, Investigation, Conceptualization. **Julia Zwara:** Investigation. **Anna Gołąbiewska:** Writing – review & editing, Writing – original draft, Validation, Conceptualization. **Tomasz Klimczuk:** Investigation. **Grzegorz Trykowski:** Investigation. **Adriana Zaleska-Medynska:** Writing – review & editing, Supervision, Project administration, Formal analysis, Conceptualization.

Declaration of competing interest

The authors declare that they have no known competing financial interests or personal relationships that could have appeared to influence the work reported in this paper.

Appendix A. Supplementary data

Supplementary data to this article can be found online at https://doi.org/10.1016/j.mssp.2022.106851.

References

[1] Y.-J. Lee, J.-K. Kang, S.-J. Park, C.-G. Lee, J.-K. Moon, P.J.J. Alvarez, Photocatalytic degradation of neonicotinoid insecticides using sulfate-doped Ag_3PO_4 with enhanced visible light activity, Chem. Eng. J. 402 (2020), 126183, https://doi.org/10.1016/j.cej.2020.126183.

[2] W. Wang, B. Cheng, J. Yu, G. Liu, W. Fan, Visible-light photocatalytic activity and deactivation mechanism of Ag_3PO_4 spherical particles, Chem.–Asian J. 7 (8) (2012) 1902–1908, https://doi.org/10.1002/asia.201200197.

[3] J. Zwara, E. Grabowska, T. Klimczuk, W. Lisowski, A. Zaleska-Medynska, Shape-dependent enhanced photocatalytic effect under visible light of Ag_3PO_4 particles, J. Photochem. Photobiol. Chem. 367 (2018) 240–252, https://doi.org/10.1016/j.jphotochem.2018.08.006.

[4] T. Bavani, J. Madhavan, S. Prasad, M.S. AlSalhi, M.J. AlJaafreh, A straightforward synthesis of visible light driven $BiFeO_3/AgVO_3$ nanocomposites with improved photocatalytic activity, Environ. Pollut. 269 (2021), 116067, https://doi.org/10.1016/j.envpol.2020.116067.

[5] T. Bavani, J. Madhavan, S. Prasad, M.S. AlSalhi, M. Aljaffreh, S.V. Anand, Fabrication of novel $AgVO_3$/BiOI nanocomposite photocatalyst with photoelectrochemical activity towards the degradation of Rhodamine B under visible light irradiation, Environ. Res. (2021), 111365, https://doi.org/10.1016/j.envres.2021.111365.

[6] D. Chen, B. Li, Q. Pu, X. Chen, G. Wen, Z. Li, Preparation of Ag-$AgVO_3$/g-C_3N_4 composite photo-catalyst and degradation characteristics of antibiotics, J. Hazard Mater. 373 (2019) 303–312, https://doi.org/10.1016/j.jhazmat.2019.03.090.

[7] W.-K. Jo, S. Kumar, P. Yadav, S. Tonda, In situ phase transformation synthesis of unique Janus Ag_2O/Ag_2CO_3 heterojunction photocatalyst with improved photocatalytic properties, Appl. Surf. Sci. 445 (2018) 555–562, https://doi.org/10.1016/j.apsusc.2018.03.194.

[8] A. Petala, A. Nasiou, D. Mantzavinos, Z. Frontistis, Photocatalytic evaluation of Ag_2CO_3 for ethylparaben degradation in different water matrices, Water 12 (4) (2020) 1180, https://doi.org/10.3390/w12041180.

[9] R.A. Senthil, A. Khan, J. Pan, S. Osman, V. Yang, T.R. Kumar, Y. Sun, X. Liu, A facile single-pot synthesis of visible-light-driven AgBr/Ag_2CO_3 composite as efficient photocatalytic material for water purification, Colloids Surf. A Physicochem. Eng. Asp. 586 (2020), 124183, https://doi.org/10.1016/j.colsurfa.2019.124183.

[10] R.A.P. Ribeiro, M.C. Oliveira, M.R.D. Bomio, S.R. de Lazaro, J. Andrés, E. Longo, Connecting the surface structure, morphology and photocatalytic activity of Ag_2O: an in depth and unified theoretical investigation, Appl. Surf. Sci. 509 (2020), 145321, https://doi.org/10.1016/j.apsusc.2020.145321.

[11] H. Xu, J. Xie, W. Jia, G. Wu, Y. Cao, The formation of visible light-driven Ag/Ag_2O photocatalyst with excellent property of photocatalytic activity and photocorrosion inhibition, J. Colloid Interface Sci. 516 (2018) 511–521, https://doi.org/10.1016/j.jcis.2018.01.071.

[12] S. Yang, D. Xu, B. Chen, B. Luo, W. Shi, In-situ synthesis of a plasmonic Ag/AgCl/Ag_2O heterostructures for degradation of ciprofloxacin, Appl. Catal. B Environ. 204 (2017) 602–610, https://doi.org/10.1016/j.apcatb.2016.10.013.

[13] Y-Cai Zhou, P. Wang, H. Fu, C. Zhao, C-Chen Wang, Ternary Ag/Ag_3PO_4/MIL-125-NH_2 Z-scheme heterojunction for boosted photocatalytic Cr(VI) cleanup under visible light, Chin. Chem. Lett. 31 (2020) 2645–2650, https://doi.org/10.1016/j.cclet.2020.02.048.

[14] Ch Gopinath, N. Nalajala, A scalable and thin film approach for solar hydrogen generation: a review on enhanced photocatalytic water splitting, J. Mater. Chem. 9 (2021) 1353–1371, https://doi.org/10.1039/D0TA09619A.

[15] D.J. Martin, G. Liu, S.J.A. Moniz, Y. Bi, A.M. Beale, J. Ye, J. Tang, Efficient visible driven photocatalyst, silver phosphate: performance, understanding and perspective, Chem. Soc. Rev. 44 (21) (2015) 7808–7828, https://doi.org/10.1039/C5CS00380F.

[16] H. Yin, Y. Cao, T. Fan, M. Zhang, J. Yao, P. Li, S. Chen, X. Liu, In situ synthesis of Ag_3PO_4/C_3N_5 Z-scheme heterojunctions with enhanced visible-light-responsive photocatalytic performance for antibiotics removal, Sci. Total Environ. 754 (2021), 141926, https://doi.org/10.1016/j.scitotenv.2020.141926.

[17] K. Ouyang, N. Jiang, W. Xue, S. Xie, Enhanced photocatalytic activities of visible light-responsive Ag_3PO_4-GO photocatalysts for oxytetracycline hydrochloride degradation, Colloids Surf. A Physicochem. Eng. Asp. 604 (2020), 125312, https://doi.org/10.1016/j.colsurfa.2020.125312.

[18] C. Mu, Y. Zhang, W. Cui, Y. Liang, Y. Zhu, Removal of bisphenol A over a separation free 3D Ag_3PO_4-graphene hydrogel via an adsorption-photocatalysis synergy, Appl. Catal. B Environ. 212 (Supplement C) (2017) 41–49, https://doi.org/10.1016/j.apcatb.2017.04.018.

[19] D. Chen, H. Feng, J. Li, Graphene oxide: preparation, functionalization, and electrochemical applications, Chem. Rev. 112 (11) (2012) 6027–6053, https://doi.org/10.1021/cr300115g.

[20] Q. Xiang, D. Lang, T. Shen, F. Liu, Graphene-modified nanosized Ag_3PO_4 photocatalysts for enhanced visible-light photocatalytic activity and stability, Appl. Catal. B Environ. 162 (2015) 196–203, https://doi.org/10.1016/j.apcatb.2014.06.051.

[21] Y. Liu, D. Yang, R. Yu, J. Qu, Y. Shi, H. Li, Z.-Z. Yu, Tetrahedral silver phosphate/graphene oxide hybrids as highly efficient visible light photocatalysts with excellent cyclic stability, J. Phys. Chem. C 121 (45) (2017) 25172–25179, https://doi.org/10.1021/acs.jpcc.7b07848.

[22] G. Chen, H. Wang, W. Dong, Y. Huang, Z. Zhao, Y. Zeng, Graphene dispersed and surface plasmon resonance-enhanced Ag3PO4 (DSPR-Ag3PO4) for visible light driven high-rate photodegradation of carbamazepine. https://doi.org/10.1016/j.cej.2020.126850, 1 February 2021, 405.

[23] B. Ohtani, Preparing articles on photocatalysis-beyond the illusions, misconceptions, and speculation, Chem. Lett. 37 (2008) 216–229.

[24] B. Jiang, Y. Wang, J.Q. Wang, C. Tian, W. Li, Q. Feng, Q. Pan, H. Fu, In situ fabrication of Ag/Ag_3PO_4/graphene triple heterostructure visible-light photocatalyst through graphene-assisted reduction strategy, ChemCatChem 5 (6) (2013) 1359–1367, https://doi.org/10.1002/cctc.201390030.

[25] M.I. Shinger, A.M. Idris, S. Devaramani, D.-D. Qin, H. Baballa, S.-T. Zhang, D.-L. Shan, X. Lu, In situ fabrication of graphene-based Ag_3PO_4@ AgBr composite with enhanced photocatalytic activity under simulated sunlight, J. Environ. Chem. Eng. 5 (2) (2017) 1526–1535, https://doi.org/10.1016/j.jece.2017.02.032.

[26] G. Chen, M. Sun, Q. Wei, Y. Zhang, B. Zhu, B. Du, Ag_3PO_4/graphene-oxide composite with remarkably enhanced visible-light-driven photocatalytic activity toward dyes in water, J. Hazard Mater. 244 (2013) 86–93, https://doi.org/10.1016/j.jhazmat.2012.11.032.

[27] W. Chen, X. Niu, J. Wang, A photocatalyst of graphene oxide (GO)/Ag_3PO_4 with excellent photocatalytic activity over decabromodiphenyl ether (BDE-209) under visible light irradiation, J. Photochem. Photobiol. Chem. 356 (2018) 304–311, https://doi.org/10.1016/j.jphotochem.2017.12.038.

[28] L. Liu, J. Liu, D.D. Sun, Graphene oxide enwrapped Ag_3PO_4 composite: towards a highly efficient and stable visible-light-induced photocatalyst for water purification, Catal. Sci. Technol. 2 (12) (2012) 2525–2532, https://doi.org/10.1039/C2CY20483E.

[29] T. Zhou, X. Huang, H. Zhang, H. Yang, K. Ma, P. Zhang, G. Zhang, Tuning the electronic structure of Ag_3PO_4-based composites through a graphene oxide mediator for enhanced photocatalytic activity, Catal. Sci. Technol. 10 (22) (2020) 7661–7670, https://doi.org/10.1039/D0CY01447H.

[30] L. Xu, Y. Wang, J. Liu, S. Han, Z. Pan, L. Gan, High-efficient visible-light photocatalyst based on graphene incorporated Ag_3PO_4 nanocomposite applicable for the degradation of a wide variety of dyes, J. Photochem. Photobiol. Chem. 340 (2017) 70–79, https://doi.org/10.1016/j.jphotochem.2017.02.022.

[31] X. Yang, H. Cui, Y. Li, J. Qin, R. Zhang, H. Tang, Fabrication of Ag_3PO_4-graphene composites with highly efficient and stable visible light photocatalytic performance, ACS Catal. 3 (3) (2013) 363–369, https://doi.org/10.1021/cs3008126.

[32] H. Lin, H. Ye, B. Xu, J. Cao, H. Chen, Ag_3PO_4 quantum dot sensitized $BiPO_4$: a novel p–n junction $Ag_3PO_4/BiPO_4$ with enhanced visible-light photocatalytic activity, Catal. Commun. 37 (2013) 55–59, https://doi.org/10.1016/j.catcom.2013.03.026.

[33] Fu-Jye Sheu, Chun-Pei Cho, Yu-Ting Liao, Chang-tze yu Ag_3PO_4 -TiO_2 -graphene oxide ternary composites with efficient photodegradation, Hydrogen Evolution, and Antibacterial Properties, Catalysts 8 (2018) 57, https://doi.org/10.1016/j.apsusc.2018.10.049.

[34] Xiaofei Yang, Haiying Cui, Li Yang, Jieling Qin, Rongxian Zhang, Hua Tang, Fabrication of Ag_3PO_4-graphene composites with highly efficient and stable visible light photocatalytic performance, ACS Catal. 3 (2013) 363–369, https://doi.org/10.1021/cs3008126.

[35] Can Cui, Yaping Wang, Dayu Liang, Wei Cui, Haihua Hu, Bingqing Lu, Sheng Xu, Xiaoyun Li, Chong Wang, Yu Yang Photo-assisted synthesis of Ag_3PO_4/reduced graphene oxide/Ag heterostructure photocatalyst with enhanced photocatalytic activity and stability under visible light, Appl. Catal. B Environ. (2014) 158–159, https://doi.org/10.1016/j.apcatb.2014.04.007, 150–160.

[36] Ma Ni, Yiwei Qiu, Yichao Zhang, Hanyang Liu, Yana Yang, Jingwei Wang, Xiaoyun Li, Can Cui Reduced graphene oxide enwrapped pinecone-liked Ag_3PO_4/TiO_2 composites with enhanced photocatalytic activity and stability under visible light, J. Alloys Compd. 648 (2015), https://doi.org/10.1016/j.jallcom.2015.07.070, 818e825.

[37] Guodong Chen, Meng Sun, Wei Qin, Yongfang Zhang, Baocun Zhu, Bin Du Ag_3PO_4/graphene oxide composite with remarkably enhanced visible-light-driven photocatalytic activity toward dyes in water, 244– 245, J. Hazard Mater. (2013) 86–93, https://doi.org/10.1016/j.jhazmat.2012.11.032.

[38] Quanjun Xiang, Di Lang, Tingting Shen, Fan Liu Graphene-modified nanosized Ag_3PO_4 photocatalysts for enhanced visible-light photocatalytic activity and stability, Appl. Catal. B Environ. 162 (2015) 196, https://doi.org/10.1016/j.apcatb.2014.06.051. –203.

[39] Lei Liu, Jincheng Liu, Darren Delai Sun Graphene oxide enwrapped Ag_3PO_4 composite: towards a highly efficient and stable visible-light-induced photocatalyst for water purification, Catal. Sci. Technol. 2 (2012) 2525–2532, https://doi.org/10.1039/C2CY20483E.

[40] Bo Chai, Li Jing, Qian Xu, Reduced graphene oxide grafted Ag_3PO_4 composites with efficient photocatalytic activity under visible-light irradiation, Ind. Eng. Chem. Res. 53 (2014), https://doi.org/10.1021/ie4041065, 8744−8752.

[41] Pengyu Dong, Yuhua Wang, Baocheng Cao, Shuangyu Xin, Linna Guo, Jia Zhang, Fenghua Li, Ag_3PO_4/reduced graphite oxide sheets nanocomposites with highly enhanced visible light photocatalytic activity and stability *Applied Catalysis B, Environmental 132– 133*, https://doi.org/10.1016/j.apcatb.2012.11.022, 2013, 45-53.

[42] Hui Xu, Cheng Wang, Yanhua Song, Jiaxiang Zhu, Yuanguo Xu, Yan Jia, Yongxiu Song, Huaming Li CNT/Ag_3PO_4 composites with highly enhanced visible light photocatalytic activity and stability, Chem. Eng. J. 241 (2014) 35–42, https://doi.org/10.1016/j.cej.2013.11.065.

[43] Q.H. Liang, Y. Shi, W.J. Ma, Z. Li, X.M. Yang, Enhanced photocatalytic activity and structural stability by hybridizing Ag_3PO_4 nanospheres with graphene oxide sheets, Phys. Chem. Chem. Phys. 14 (2012) 15657–15665, https://doi.org/10.1039/C2CP42465G.

[44] C. Cui, Y.P. Wang, D.Y. Liang, W. Cui, H.H. Hu, B.Q. Lu, S. Xu, X.Y. Li, C. Wang, Y. Yang, Photo-assisted synthesis of Ag_3PO_4/reduced graphene oxide/Ag heterostructure photocatalyst with enhanced photocatalytic activity and stability under visible light, Appl. Catal. B Environ. 158 (2014) 150–160, https://doi.org/10.1016/j.apcatb.2014.04.007.

[45] Pengyu Dong, Guihua Hou, Chao Liu, Xinjiang Zhang, Hao Tian, Fenghua Xu, Xinguo Xi, Rong Shao, Origin of activity and stability enhancement for Ag_3PO_4 photocatalyst after calcination, Materials 9 (2016) 968, https://doi.org/10.3390/ma9120968, https://doi.org/10.3390/ma9120968.

[46] K. A. Shiral Fernando, Venroy G. Watson, Xifan Wang, Nicholas D. McNamara, Mary C. JoChum, Dylan W. Bair, Barbara A. Miller, and Christopher E. Bunker, Migration of silver nanoparticles from silver decorated graphene oxide to other carbon nanostructures Am. Chem. Soc. dx.doi.org/10.1021/la502401n.
[47] Yong Han Jerome Leow, Patria Yun Xuan Lim, Sharon Xiaodai Lim, Jianfeng Wu, Chorng-Haur Sow, Nanosurfer flash-mobs: electric-field-choreographed silver migration on graphene oxide, Nanoscale Adv. 1 (2019) 2180, https://doi.org/10.1039/c9na00151d.
[48] Wenguang Wan, Bei Cheng, Jiaguo Yu, Gang Liu, Wenhong Fan, *Visible-light photocatalytic Activity and deactivation Mechanism of Ag_3PO_4 spherical particles*, 00, 0 – 0, Chem. Asian J. (2012), https://doi.org/10.1002/asia.201200197.
[49] Shaoqing Song, Aiyun Meng, Shujuan Jiang, Bei Cheng, Three-dimensional hollow graphene efficiently promotes electrontransfer of Ag_3PO_4 for photocatalytically eliminating phenol, Appl. Surf. Sci. 442 (2018) 224, https://doi.org/10.1016/j.apsusc.2018.02.102.